Engineering Failure Analysis 143 (2023) 106841

Contents lists available at ScienceDirect

Engineering Failure Analysis

journal homepage: www.elsevier.com/locate/engfailanal

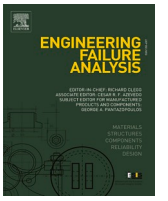

Engineering and analyses of a novel Catalan vault

V. Savino, M. Franciosi, M. Viviani *

School of Engineering and Management Vaud, HES-SO University of Applied Sciences and Arts Western Switzerland

ARTICLE INFO

Keywords:
Catalan vaults
Ecorasilla
FE analyses
Rasillas
Sustainable construction materials
Vaults failure

ABSTRACT

Among the techniques for constructing vaults without formwork, the most popular is the Catalan. The first layer of lightweight tiles called "Rasillas" is assembled to form a predeterminate shape that resist to loads despite its reduced thickness. Until the first layer is completed, a sticky, quick setting mortar supports the terracotta tiles. Once completed, the first layer of the vault acts as a temporary formwork to support the further layers of tiles and then become a part of the structure. This paper presents a numerical analysis of the mechanical behavior of a novel type of Catalan vault made of sustainable raw excavation-earth tiles called "Ecorasillas". The advantages and drawbacks of the Ecorasilla vaults are highlighted and their performances are compared with a second type of Catalan vault made of clinker bricks. Test results are used to improve the quality of the predictions of the FEM models.

1. Introduction

Whereas Catalan vaults are often considered a type of structure, the term "Catalan" refers to an ordinary vault constructed with a particular technique. This technique permits to build vaults without the use of formwork. This is possible thanks to the use of light-weight bricks and a rapid set jointing mortar bonding bricks together [1]. The idea of constructing vaults without formwork is very ancient [2]. The adobe masonry barrel vaults founded in Egypt were constructed with mud-bricks slightly laid to the vertical such that the formwork, also called center, was not necessary [2]. The cunning idea of constructing vaults without a center of the ancient masons was improved and modified along the centuries. One of the most interesting examples of evolution of the technique is the octagonal dome of Santa Maria Del Fiore in Florence [3]. The construction was much delayed due to the fact that building a center proved to be impossible. In 1420 Brunelleschi's original *spina pesci* technique finally permitted the construction of the dome without a center. The Catalan technique has been popularized all over the world by Gaudi and by Guastavino. Both pioneers introduced the idea of using standardized thin tiles and layers of Portland cement mortar. Vaults are structures that, due to their form, are essentially compressed. Vaults can be constructed with sustainable materials in most regions of the world, also in seismic ones [4]. At the present times, Catalan vaults are still constructed by firstly building a self-supporting layer without center. Once the first layer is completed, it functions as a center for further layers of bricks (usually variable between one and three) that are laid by rotating their joints with respect to the previous layer, ideally of 45°. The last layer of the vault might be thicker than the other ones if an extra load bearing capacity of the whole structure is desired. In the case of reinforced Catalan vaults [5], before the last layer, a grid made of steel, GFRP or other materials, can be embedded in the mortar connecting the layers. This grid is as thin as possible and has the purpose of reinforcing the mortar rather than distributing the concentrated loads, whose effect on the mechanical response of the vault are presented in the work of Lopez et. al. 2012 [6]. Nowadays merging the traditional Catalan vaulting technique with the use of ecological earth-based materials

* Corresponding author.
E-mail address: marco.viviani@heig-vd.ch (M. Viviani).

https://doi.org/10.1016/j.engfailanal.2022.106841
Received 19 April 2022; Received in revised form 22 September 2022; Accepted 26 September 2022
Available online 2 October 2022

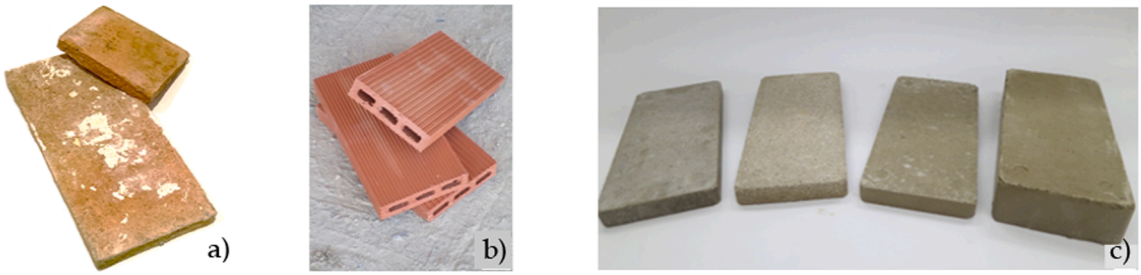

Fig. 1. Traditional terracotta "rasilla" (a), modern terracotta "rasilla" (b) and different types of Ecorasilla made with different excavation earth and different stabilizers (c).

is of great interest not only to meet architectural and aesthetic requirements but also to increase the sustainability of the whole construction market. The disposal of the excavation earth is one of the major worldwide issues of the construction waste management. In Switzerland, each year, 18 million tons of non-polluted earth are excavated, most of which are landfilled. The idea of converting this waste into a construction material is studied in many countries [7]. Two of the most efficient solutions to convert the excavated earth into a construction material are i) to produce compressed earth bricks [8] and ii) to produce Shot-Earth [7,9,10]. The earth might be stabilized by instance with cement or lime. In some cases, according to the application and the nature of the excavated earth, the stabilization might be abandoned. Most of the times, modern excavation earth bricks are stabilized to regularize their mechanical properties and to reduce their sensibility to water [11]. In recent years the rising interest in Catalan vaults has prompted the construction companies and the researchers to propose compressed earth bricks also for Catalan vaults. The brick originally used to construct Catalan vaults is the "rasilla" a thin terracotta tile, see Fig. 1. In this work, a more ecological version of rasilla has been developed for building a novel type of Catalan vault, see Fig. 1c. The name "Ecorasilla" is used to describe a thin tile composed mainly by the excavation earth dug from a construction site, water and a low amount of stabilizer [12]. Consequently, the performances of the Catalan vaults built with an Ecorasillas masonry depends on the properties of the raw materials. In addition, the properties of the excavated earth vary from an excavation site to another. Thus, a comprehensive understanding of the mechanical response of Ecorasillas vaults demands a thorough mechanical characterization of this sustainable building material.

In the design of barrel vaults the safety of the structure during construction under uniform gravity loads can be verified via the membrane theory. The membrane theory assumes that no bending stresses occur and that all forces are carried along the center-line surface of the domes, by combining meridional and hoop forces [13,14]. For asymmetrical live loading on the domes, the use of graphic static permits to search for equilibrium solutions. The graphic static also permits to determine the structure shape via assumptions on the geometry and the internal actions [15]. Due to the flexibility of the masonry technique, changes of shape are possible also during the early construction steps [16]. Standard design software does not permit to modify the path of the internal action as the shape of the vault and loads are inputs data, while the internal actions are output information [17]. However, the so-called dynamic geometric software like Geogebra, permits to perform geometric constructions by saving the parametric relationship between the objects. For example, if the position of the free nodal elements of the structure (or nodal loads) is changed, the internal actions and the geometry are automatically updated [17]. Consequently, the dynamic geometry feature can be used to perform graphic static analyses. However, this kind of software integrates only the geometrical boundaries and therefore the construction of the graphic static model is done manually by the designer. Advancement toward the development of interactive graphic static methods can be found in literature [18,19].

Today the analysis of Catalan vaults is commonly performed via finite element methods (FEMs). With this methodology the masonry is modeled as a continuum material with certain elastic properties [20]. Catalan vaults are traditionally made by layers of bonded bricks intercalated with a mortar. Thus, for a more accurate analysis, it should be implemented a series of computational parameters accounting for the layered and heterogeneous nature of the masonry [21,22]. FEM method is not always the best choice for the structural design of Catalan vaults. The main reason is that the numerical analyses also depend on the assumptions made on the masonry and its components properties, on the scale effect [23] and on the characteristics of the supporting elements of the vaults. These assumptions, coupled with the principles of static equilibrium, permit nevertheless to write a system of equations with a unique solution, strongly dependent by the above-mentioned assumptions [24]. To reduce the impact of these assumptions, researchers have proposed a semi-inverse analysis of full-scale test data by iteratively calibrating the elastic properties of both the materials and the structural elements of the Catalan vaults [25].

The aim of the present work is twofold: (i) highlight the benefits and drawbacks of Ecorasilla Catalan vaults and (ii) improve the quality of the FEM analysis of the Ecorasilla vaults by taking into account the results of experimental tests carried out on macro-elements made with the same Ecorasilla masonry used to construct the sustainable Catalan vaults. Results of tests in masonry components (bricks and mortar) are also used.

Fig. 2. Hydraulic static compaction device making earth-based brick like Ecorasillas.

Table 1
Analysis strategy.

Masonry type	Experimental analysis					FEM analysis		
	Testing configuration		Load direction	Number of samples	Dimensions (mm)	Model configuration		Dimensions (mm)
M−FB[1)]	Masonry units	M−FB−UC[2)]	L[3)]	3	145 × 360 × 360	–		
		M−FB−BF[2)]	–	3	–			
		M−FB−YM[2)]	–	3	–			
	Macro samples	M−FB−W[4)]	–	3	145 × 800 × 800			
		M−FB−D[4)]	–	3	145 × 800 × 800			
		M−FB−S[4)]	–	3	145 × 800 × 800			
M−ER[1)]	Masonry units	M−ER−UC[2)]	//[3)]	3	80 × 130 × 260	–		
			L[3)]	3	80 × 130 × 260			
			plan[3)]	3	80 × 130 × 260			
		M−ER−BF[2)]	–	3	20 × 130 × 260			
		M−ER−YM[2)]	–	3	80 × 130 × 260			
	Macro samples	M−ER−W[4)]	–	3	120 × 1000 × 1000	Macro samples	H-FEM[5)] (Adina)	120 × 1000 × 1000
		M−ER−D[4)]	–	3	120 × 1000 × 1000		ML-FEM[6)] (Adina)	120 × 1000 × 1000
		M−ER−S[4)]	–	3	120 × 1000 × 1000	Full structure	H-FEM[5)] (SCIA)	see Table 5

[1)] M: masonry; FB: clinker brick; ER: Ecorasillas brick;
[2)] UC: uniaxial compression test; BF: bending flexural test; YM: Young's modulus test;
[3)] //, L, plan: Loading directions, see Fig. 4;
[4)] W: compression test on wall; D: lateral compression test on wall; S: energy adsorption test on slab;
[5)] H-FEM: finite element model assuming the masonry as an idealized homogenous material;
[6)] ML-FEM: finite element model assuming the masonry as realistic multi-layer material;

2. Experimental campaign

2.1. Materials

2.1.1. Ecorasillas masonry (M−ER)

Ecorasillas tiles (labeled hereafter M−ER) are typically manufactured by mixing two volumes of crushed earth, with one volume of river sand 0/4 mm and a low amount (from 0 to 12 % by weight) of cement as stabilizer. The crushed earth used in this study is collected from an excavation site at Ault (France). It is commonly referred in the area as a chalky earth or simply as chalk [26]. The cement used is a commercial OPC cement (CEM I 42.5 N). Studies have shown that the Proctor optimum moisture content increases and dry bulk density decreases when the earth is stabilized [27]. All materials are mixed together for a couple of minutes in a standard concrete mixer. Then, the fresh mixture is compacted via a hydraulic static device, see Fig. 2, with a compacting pressure of 0.01 MPa. The compacting load acts vertically on a prismatic mold. The final dimensions of the Ecorasillas (ER) are 20 × 130 × 260 mm. The

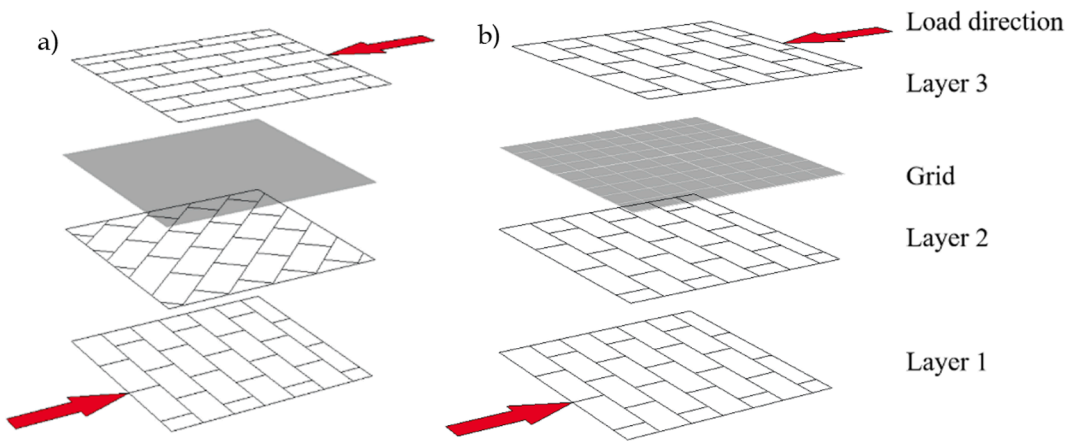

Fig. 3. Layer order of bricks in (a) M−ER−W and (b) M−FB−W samples, mortar layers between bricks are not illustrated. In M−ER−W the grid is composed by GFRP, in M−FB−W the grid is a thin steel mesh. Load direction is not representative for all tests conducted.

compaction process to produce one ER takes 20 s. The low moisture rate used in the mix enables an optimal compaction rate and the production of a sound ER. The surface of the press is usually warmed in order to simplify the brick removal. Once extracted from the press, the fresh ER are stored under a tarpaulin during one week under controlled conditions (20 ± 2 °C, RH 55 ± 10 %). Then, the bricks are let dry for three weeks. A specific mortar is used to bond the first layer of the Catalan vaults. Sticky consistency and quick setting time are requested for the mortar of the first layer. For reaching both requirements the mix design of the mortar is composed by plaster:hydrated lime:sand 30:20:50 by weight. The first layer of bricks and hardened mortar plays the role of a formwork (center) for assembling the superior layers. With the exception of the first layer, the other ones are bonded using a commercial M5 Portland cement-based mortar. The interlayer mortar thickness is about 10 mm.

2.1.2. Clinker brick masonry (M−FB)

The second type of masonry investigated in this campaign is made of commercial high strength clinker bricks (labeled here after M−FB). This commercial brick has dimensions of 40 × 115 × 365 mm and is produced in agreement with the European standards [28]. Thanks to the process of clinkerization the bricks reach a weight of 2200 kg/m^3, 44 MPa of compression strength and a fire resistance of type A1, as reported in the producer's datasheet. The mortar used to assembly M−FB is a commercial M5 Portland cement-based mortar.

2.2. Experimental testing

In order to properly analyze the mechanical response of the M−ER Catalan vault, an experimental investigation which takes into account the properties of masonry elements as well as the scale effect is a priority. Tests on *meso*-scale samples composed of few bricks are useful to compare ER properties with known materials. But, in the interest of the second purpose of the work, test results will suffer of a scale effect bias. For this reason, this work also includes an experimental investigation on the mechanical properties of macro-scale samples (walls and slabs), whose dimensions are found in Table 1. All samples mentioned in Table 1 are fabricated with the traditional Catalan technique presented in Sections 1, 2.1 and in Fig. 3a. In this study, M−ER is made of three layers of ER. In the third layer the ERs has a double thickness. A GFRP mesh [5] is embedded between the second and the third layer to reinforce the mortar and to improve the mechanical response of the vaults against local loading [29]. Samples of M−FB are fabricated by a company specialized in masonry construction. The typical steps of the Catalan technique are used, see Sections 1, 2.1 and in Fig. 3b, with one exception: the three layers of bricks are superimposed and placed along the same direction (see Fig. 3b) such that, in one direction, bonds are parallel for all the three layers. A thin galvanized steel hexagonal mesh is embedded between the second and the third layer to reinforce the mortar.

Macro- and *meso*-scale samples have a realistic thickness to build the vault: 80 mm for M−ER and 145 mm for M−FB (see Table 1). The analysis of mechanical properties recorded by stressing the masonry units (*meso* scale samples) represents the first step to efficiently calibrate a finite element model of a novel Catalan vault. The analysis on macro samples serves to improves the calibration accuracy and to limit both the scale effect and the uncertainties related to the assumption on the support conditions. A displacement controlled computerized universal testing machine is used to measure the elastic response of both masonry units (*meso* scale samples) and macro samples. Uniaxial compression (UC), bending flexural (BF) and Young's modulus (YM) tests are carried out on units of M−ER. The mechanical properties of masonry units of M−FB are provided by the producer, while UC tests are carried out on M−FB *meso*-scale samples. Compression tests are performed on wall (W), lateral compression tests are performed on walls (D) and energy adsorption tests are performed on slabs (S). Table 1 summarizes the several steps of analysis accomplished in this work.

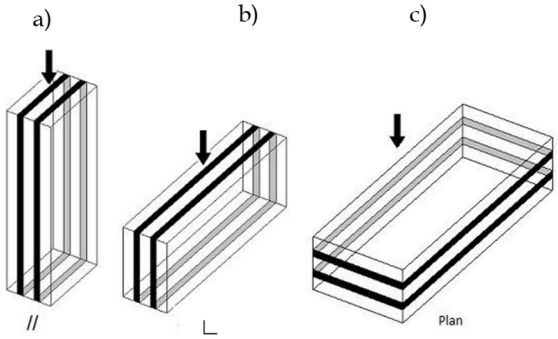

Fig. 4. Load direction setup for testing M−ER−UC and M−FB−UC samples composed of three layers of bricks with two layers of mortar.

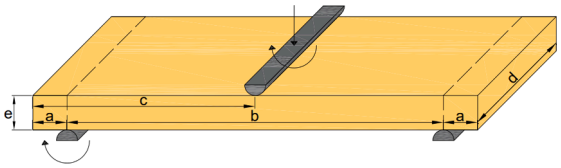

Fig. 5. Three point bending flexural test setup.

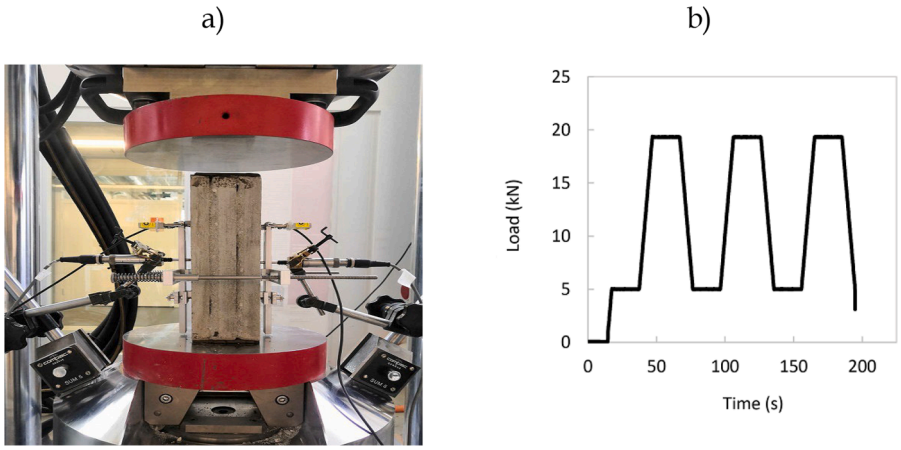

Fig. 6. Young's modulus testing on (a) M−ER−UC, (b) Loading cycles.

2.2.1. *Mechanical characterization on masonry unit*

2.2.1.1. Uniaxial compression test (UC). Compression test on masonry units of both M−ER and M−FB are conducted in agreement to the French standard for earth blocks [30]. After 14 days of curing under laboratory conditions (20 ± 2 °C, RH 55 ± 10 %) samples are ready to be tested. The speed test of UC is set to 0.15 MPa/s. The test is interrupted as soon as the failure is detected. The compression strength f_c is measured as the ratio between the mean maximum load measured on three samples of the same series and the crossing area of the sample:

$$f_c = \frac{F}{A} \tag{1}$$

where F and A are the maximum compression load acting on the sample (N) and the crossing area of the sample (mm^2), respectively.

The slenderness ratio of M−ER as well as the effect of anisotropy on the compression strength are highlighted by testing the masonry units according to three different loading orientations [31], see Fig. 4. Three M−ER samples for each loading direction are tested. As can be observed in Fig. 4, the cross section changes according to the orientation of the masonry and the loading direction. Since the mechanical properties of M−FB are provided by the producers, only the test schematized in Fig. 4b is considered for UC.

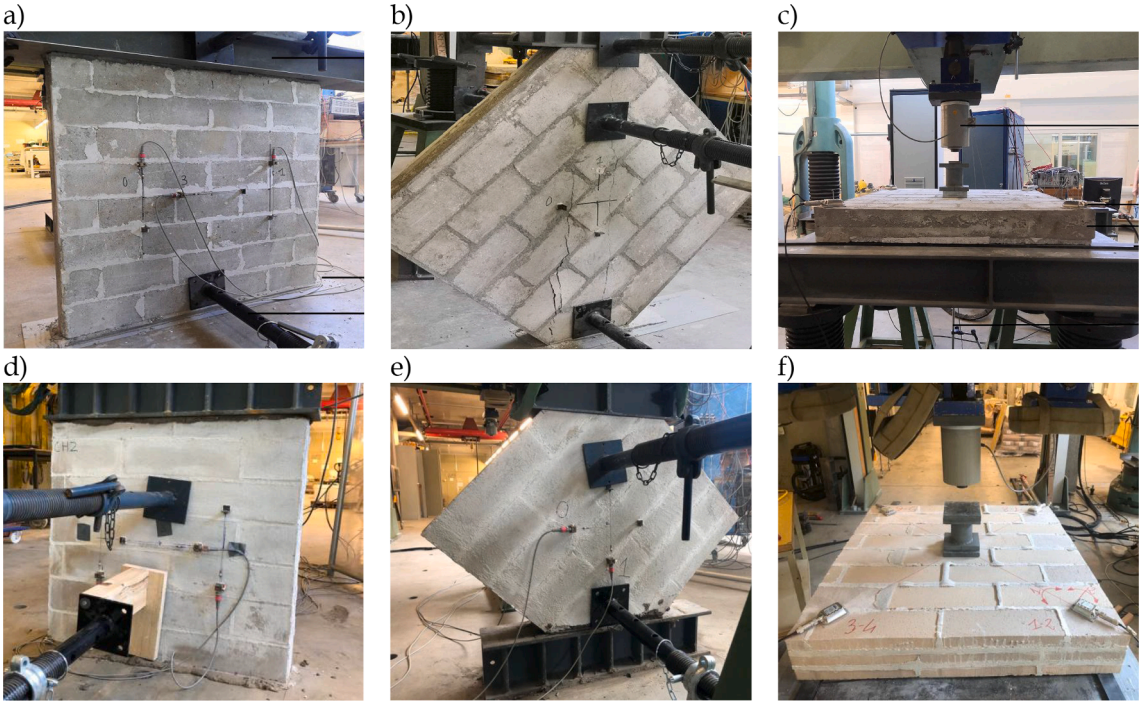

Fig. 7. Mechanical test on macro samples: (a, d) compression test on M−ER−W, M−FB−W, (b, e) diagonal compression test on M−ER−D, M−FB−D, (c, f) energy absorption test on M−ER−S, M−FB−S, respectively.

2.2.1.2. Three point bending flexural test on Ecorasillas brick (BF). In order to measure the tensile strength of M−ER, a three-point bending flexural test is carried out according to the European standards [32]. The setup layout is showed in Fig. 5. The dimensions a, b, c, d, e correspond to 20 mm, 220 mm, 125 mm, 130 mm and 20 mm respectively. The loading rate is set to 0.15 MPa/s. The test is interrupted as soon as the total failure occurs. The indirect tensile strength f_t is computed according to the following equation:

$$f_t = \frac{3}{2}\frac{F_c b}{de^2} \tag{2}$$

where F_c, b, d and e are the maximum load measured (N), the span (mm), the width (mm) and the thickness of the M−ER brick (mm).

2.2.1.3. Young's modulus test (YM). A direct measure of the Young's modulus of M−ER samples is obtained by testing three samples of masonry units. The YM has been measured according to the European standard [33], see Fig. 6. This standard for concrete has been followed since Ecorasillas tiles are more similar to the concrete in terms of composition and mixing method than masonry. The compression strength measured on M−ER−UC is used to define the maximum and the minimum loading magnitude during the three loading/unloading cycle [33], see Fig. 6b. In order to avoid any geometrical discrepancy between the UC and YM tests the dimensions of M−ER−YM and M−ER−UC samples are the same. The loading rate is set to 0.15 MPa/s. During the three cycles loading, a strain gauge (sensitivity ± 0.0005 mm), measures the average vertical strain of the middle region of the sample, see Fig. 6b. The extensometer is fixed on the brick surface away from the interfacial mortar-brick layer in order to avoid undesirable slip. The elastic modulus is computed as the mean value obtained after each cycle, for a total of three cycles [33].

2.2.2. Mechanical characterization of macro samples of the materials/assembly composing the Catalan vault

2.2.2.1. Compression test on masonry wall (W). Three macro samples of both M−ER and M−FB are manufactured, cured under laboratory conditions (20 ± 2 °C, 55 ± 10 % HR) and then subjected to axial load, see Fig. 7a and d. M−ER−W and M−FB−W samples are made by adopting the same constructive method used for masonry units, see Section 2.1.1.

The wall dimensions of both M−ER−W and M−FB−W samples are summarized in Table 1. M−ER−W and M−FB−W tests permit to analyze the elastic properties of masonry here investigated more accurately than testing *meso*-scale samples. On one hand, this permits to reduce the influence of the scale size effect. On the other hand, the boundary conditions governing the mechanical test of macro samples are closer to those of full-scale structures [16,23]. The latter plays a key role in the model calibration step (see Sections 2 and 3). In order to protect the strain gauge glued to the sample from brittle failure, horizontal props are placed on both side of the sample with no contact. The same configuration can be observed in diagonal compression test described in Section 2.2.2.2.

The testing machine consists in a servo-hydraulic high-speed test system equipped of several actuators mounted on an upper

crosshead. The actuator stroke is 330 mm plus 70 mm cushioning on each side. A system of high responsive servo valves is attached on the actuator minimizing the hydraulic pressure fluctuations. The system incorporates a load measurement and data acquisition device. Fig. 7a and d show the quasi-static compression loading test carried out on both M−ER−W and M−FB−W, respectively. The loading rate is set to 0.5 ± 0.01 mm/min. The direction of the load is showed in Figs. 6 and 7a, 7b. A series of linear variable differential transformers (LVDT) with an accuracy of ± 0,2 mm and a gauge length of 250 mm are placed on both sides of the wall in order to compute the vertical and horizontal strain, see Fig. 7a, d. The testing equipment has been adapted to properly measure the compression strength, the Young's modulus and the Poisson's ratio. The compression strength is measured as the ratio between the maximum load detected prior to reach the total failure and the crossing area of the wall, see also Eq. (1). The Young's modulus and Poisson's ratio are calculated for an interval between 10 and 30 % of the compression strength measured in the same test:

$$E_{1/3} = \frac{\Delta\sigma}{\Delta\varepsilon_v} = \frac{\sigma_{0.3} - \sigma_{0.1}}{\varepsilon_{v0.3} - \varepsilon_{v0.1}} \tag{3}$$

$$\nu_{1/3} = -\frac{\Delta\varepsilon_h}{\Delta\varepsilon_v} = \frac{\varepsilon_{h0.3} - \varepsilon_{h0.1}}{\varepsilon_{v0.3} - \varepsilon_{v0.1}} \tag{4}$$

where $\sigma_{0.1}$, $\sigma_{0.3}$, $\varepsilon_{v0.1}$, $\varepsilon_{v0.3}$, $\varepsilon_{h0.1}$, $\varepsilon_{h0.3}$, are the compression stresses, the vertical strains and the horizontal strains measured on the wall at 10 and 30 % of the compression strength, respectively. The strain value corresponds to the average magnitude measured by LVDTs placed on both sides of the wall.

2.2.2.2. Diagonal compression test on masonry wall (D). In order to measure the shear modulus of M−ER and M−FB, a diagonal compression test is performed on three macro samples for both series, labeled hereafter M−ER−D, M−FB−D. The wall dimensions of both M−ER−D and M−FB−D samples are summarized in Table 1. The walls are cut to their opposite edge and turned by 45° prior to be tested, according to the standard [34], see Fig. 7b and e. The surface loading area of M−ER−D and M−FB−D samples is 120 × 300 mm and 145 × 300 mm, respectively. Instead the vertical plane dimensions before cutting are 1000 × 1000 and 80 × 80 mm, respectively. The testing equipment is presented in the Section 2.2.4. Two LVDTs are placed along the diagonals of both sides of the samples. The loading rate is set to 0.5 ± 0.01 mm/min. The shear modulus is calculated for an interval between 10 and 30 % of the shear strength measured in the same test:

$$\begin{aligned} G_{1/3} &= \frac{\Delta\tau}{\Delta\gamma} = \frac{\tau_{0.3} - \tau_{0.1}}{\gamma_{0.3} - \gamma_{0.1}} \\ \tau &= \frac{F}{A_s} \\ \gamma &= \frac{\Delta x}{L} + \frac{\Delta y}{L} \end{aligned} \tag{5}$$

Where $\tau_{0.1}$, $\tau_{0.3}$, $\gamma_{0.1}$, $\gamma_{0.3}$, are the shear stresses and the shear strains measured on the wall at 10 and 30 % of the shear strength, respectively. While Δx, Δy, L, τ, F, A_s are the horizontal and vertical displacements measured on the wall, the characteristic length of the LVDT, the average shear stress, the load magnitude acting on the wall and the shear cross section, respectively.

2.2.2.3. Energy absorption test on masonry slab (S). Energy absorption tests are carried out to effectively measure the fracture energy G_m of M−ER and M−FB against an increasing local load applied at the center of the slab. G_m is measured by integrating the area under the path load – vertical displacement measured in the experiment. From a mechanical point of view, this information permits to highlight the role of the reinforcing mesh embedded in the masonry as well as the effect of crossing the layers of bricks and the mechanical properties of the latter. The test equipment, already presented in Sections 2.2.2.1 and 2.2.2.2, is integrated by a supporting steel frame for placing macro samples, see Fig. 7f. Three macro samples of both M−ER and M−FB are manufactured, cured under laboratory conditions (20 ± 2 °C, 55 ± 10 % HR) and then tested. Samples are labeled M−ER−S, M−FB−S, respectively. The dimensions of both M−ER−S and M−FB−S samples are summarized in Table 1. It should be mentioned that the color texture of M−FB changes from one side to the other one, but the material properties are the same. A stiff elastomer rubber is used to diffuse stress between the supporting frame and the slab bottom without affecting the mechanical response in terms of load – midspan vertical displacement, see Fig. 7c and 7f. A 200 mm strain gauge (sensitivity ± 0,2 mm) is placed on the bottom side of the slab at the midspan in order to measure the deflection. In addition, inclinometers are placed along the diagonals at the corners of the slab. The loading rate is set to 0.5 ± 0.01 mm/min.

3. Modeling

The structural performance of a new type of Catalan vault based on Ecorasillas masonry is simulated by means of a Finite-Element-Model (FEM). Two different FEM approaches can be adopted for this purpose. In the first one, the masonry material is modeled as a homogenous single component. In the second one mortar and brick layers are separately modeled considering perfect adhesion between them. The commercial software ADINA [35] is used in this work to model macro samples according to both homogenous (H-FEM) and multi-layered (ML-FEM) approaches. The engineering properties measured on masonry units, presented in Section 2.2.1, are used to calibrate the model simulating the compression test on masonry walls. A comparison between FEM analyses and experimental

Table 2
Engineering properties used for H-FEM-M-ER-W calibration after the optimization process.

Elastic Modulus	Em	8000 MPa
Poisson's ratio	ν	0.3
Shear modulus	Gm	1150 MPa
Volume weight of the masonry	ρ	1830 kg/m3

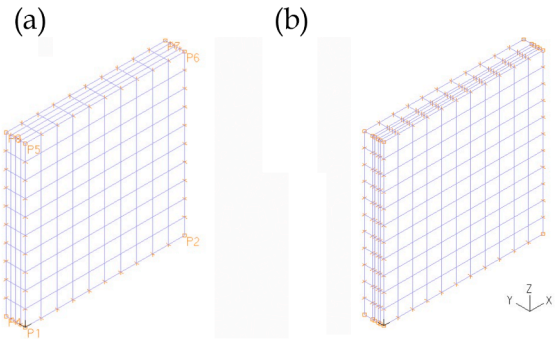

Fig. 8. (a) H-FEM-M-ER-W 3D-volume divided into 400 hexahedral-shaped 3D elements, (b) ML-FEM-M-ER-W mesh density.

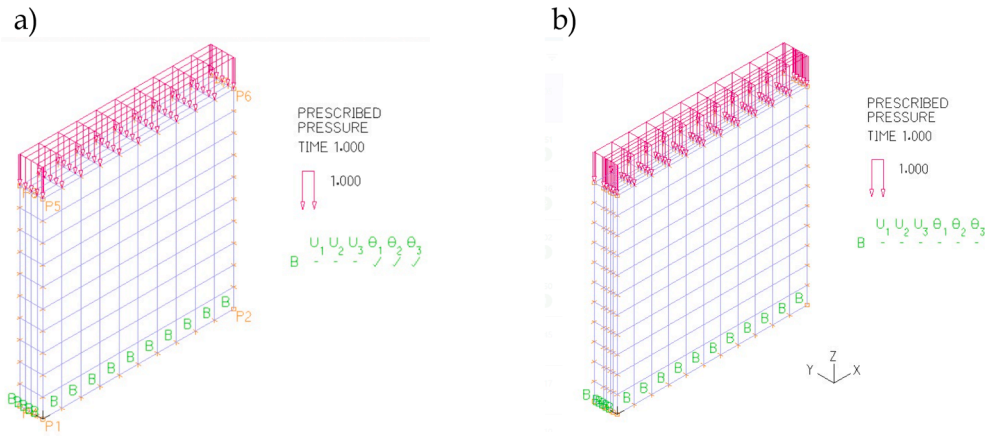

Fig. 9. Restrain and loading conditions: (a) H-FEM-M-ER-W, (b) ML-FEM-M-ER-W.

Table 3
Engineering properties used for ML-FEM-M-ER-W calibration.

Type of element	E_m	ν	ρ
	MPa	-	kg/m^3
M−ER	8300	0.3	1800
Mortar (for M−ER)	10,000	0.2	1900

results highlights the limitations of calibrating the engineering properties of a layered masonry vault only on the basis of tests carried out on no-representative (*meso*) samples. The accuracy of the model's prediction is then optimized using the engineering properties measured on representative (macro) samples, like the walls presented in Section 2.2.2.1. Results of homogenous and multi-layered (ML-FEM) approaches are compared and finally, the mechanical response of ER Catalan vault is analyzed via the commercial software SCIA Engineering [36].

3.1. Homogeneous FE model

An ideal homogenous material is assumed to simulate the mechanical response of an Ecorasillas masonry subjected to compression loads. This first model is labeled H-FEM-M-ER-W. The engineering properties governing the mechanical response of H-FEM-M-ER-W

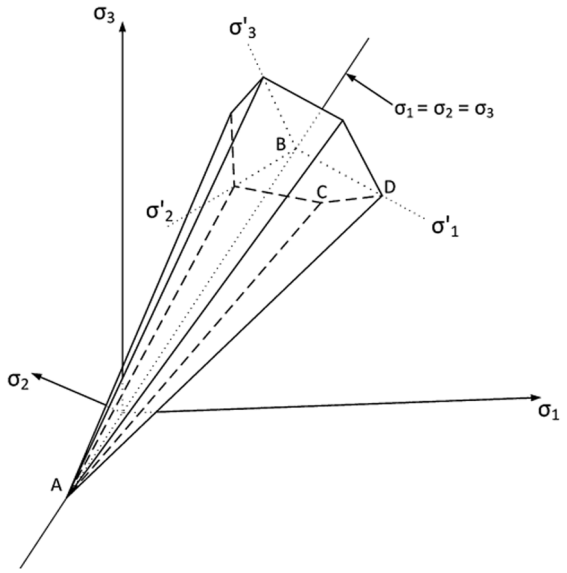

Fig. 10. Mohr–Coulomb failure surface in principal stress space.

Table 4
Material characteristics implemented for non-linear analysis in H-FEM.

E_m	G_m	ν	f_c	f_b	ρ	G_f
MPa	MPa	–	MPa	MPa	kg/m^3	N/m
8000	1150	0,3	5,6	2,6	1830	156

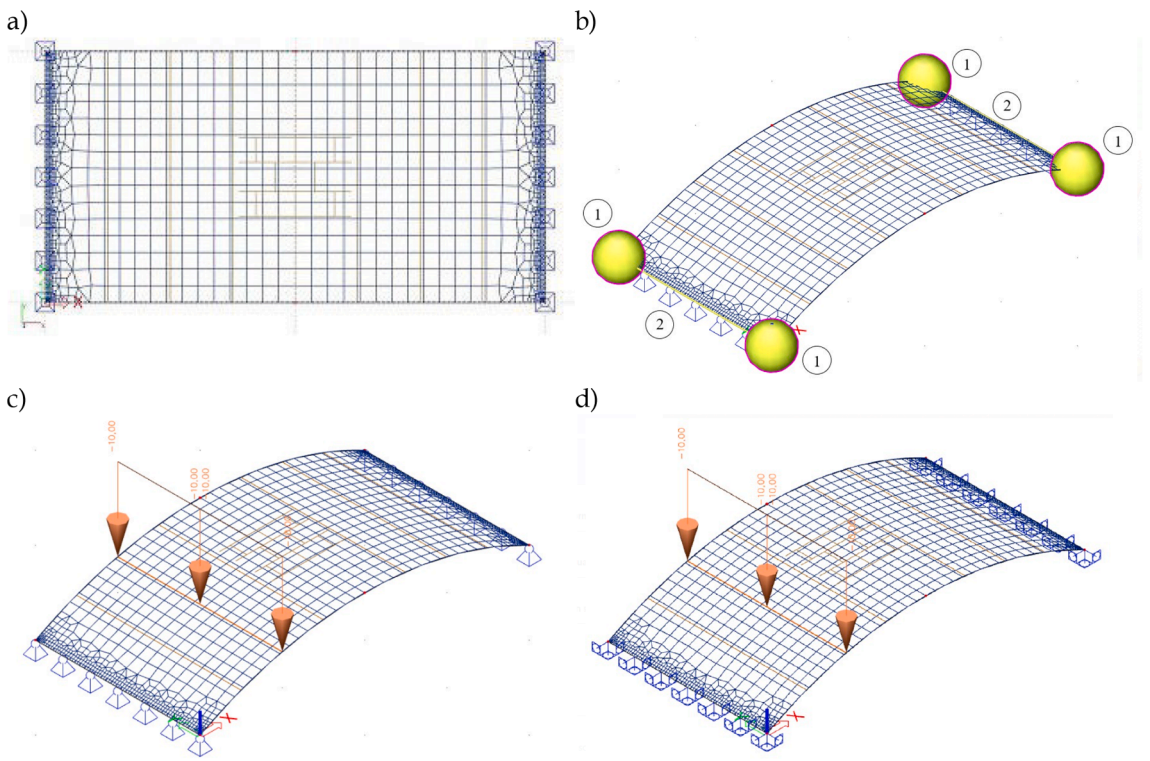

Fig. 11. (a) Mesh refinement for FE vault and (b) restrain conditions for (c) H-FEM-A-H and (d) H-FEM-A-F.

Table 5
Geometric parameters of FE vault.

Total length of the curved vault	LV	4,16 *m*
Shorter distance between the two vault supports	LP	4 *m*
Volume weight of the masonry	ρM	1830 kg/m^3
Width	b	2 *m*
Thickness	h	0,120 *m*
Radius of the curved line	R	4,25 *m*

Table 6
Experimental results.

Type of element	E_m	G_m	ν	f_c	f_t	f_b	ρ	G_f	Reference
	MPa	MPa	-	MPa	MPa	MPa	kg/m^3	N/m	
Clinker brick	3200	–	0,15	5,9	0,24	–	1219	–	[38]
Clinker brick masonry	1700	–	0,25	2,3	0,08	–	–	–	[39]
Clinker brick masonry	7400	–	0,26	14,19	1,98	0,62	1764	–	[6]
WC* clinker brick (1)	168	–	0,213	4,64	–	–	1612	–	[40]
WC* clinker brick (2)	133	–	0,211	6,18	–	–	1707	–	[40]
Earth brick masonry	533–1333	–	–	1,5 – 2,24	–	–	–	–	[41]
Earth block masonry	315	–	–	2,15	–		1870	–	[42]
Stabilized earth brick	972–1805	–	–	–	–	–	–	–	[43]
M−ER	8300	–	–	6/5,6/8	–	2.6	1800	–	Present work
Mortar (for M−FB)	–	–	–	>15		> 4			Present work
M−ER−W/M−ER−D	8000 ± 280	1150 ± 212	0,3 ± 0,0	5,6 ± 0,2	–	–	1830	156	Present work
M−FB−W/M−FB−D	6660 ± 930	6060	0,12	36,2 ± 1,15	–	–	2040	2657	Present work

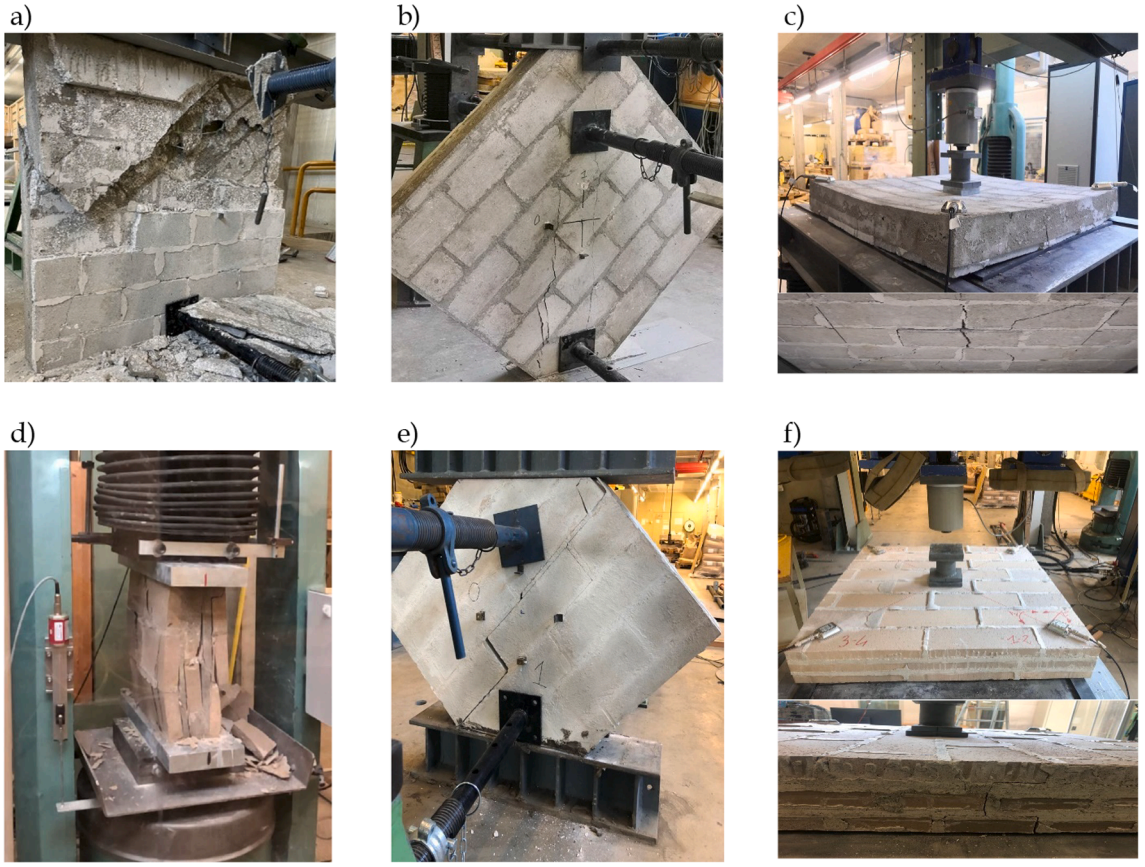

Fig. 12. Failure pattern on macro samples: (a, d) compression test on M−ER−W, M−FB−W, (b, e) diagonal compression test on M−ER−D, M−FB−D, (c, f) energy absorption test on M−ER−S, M−FB−S.

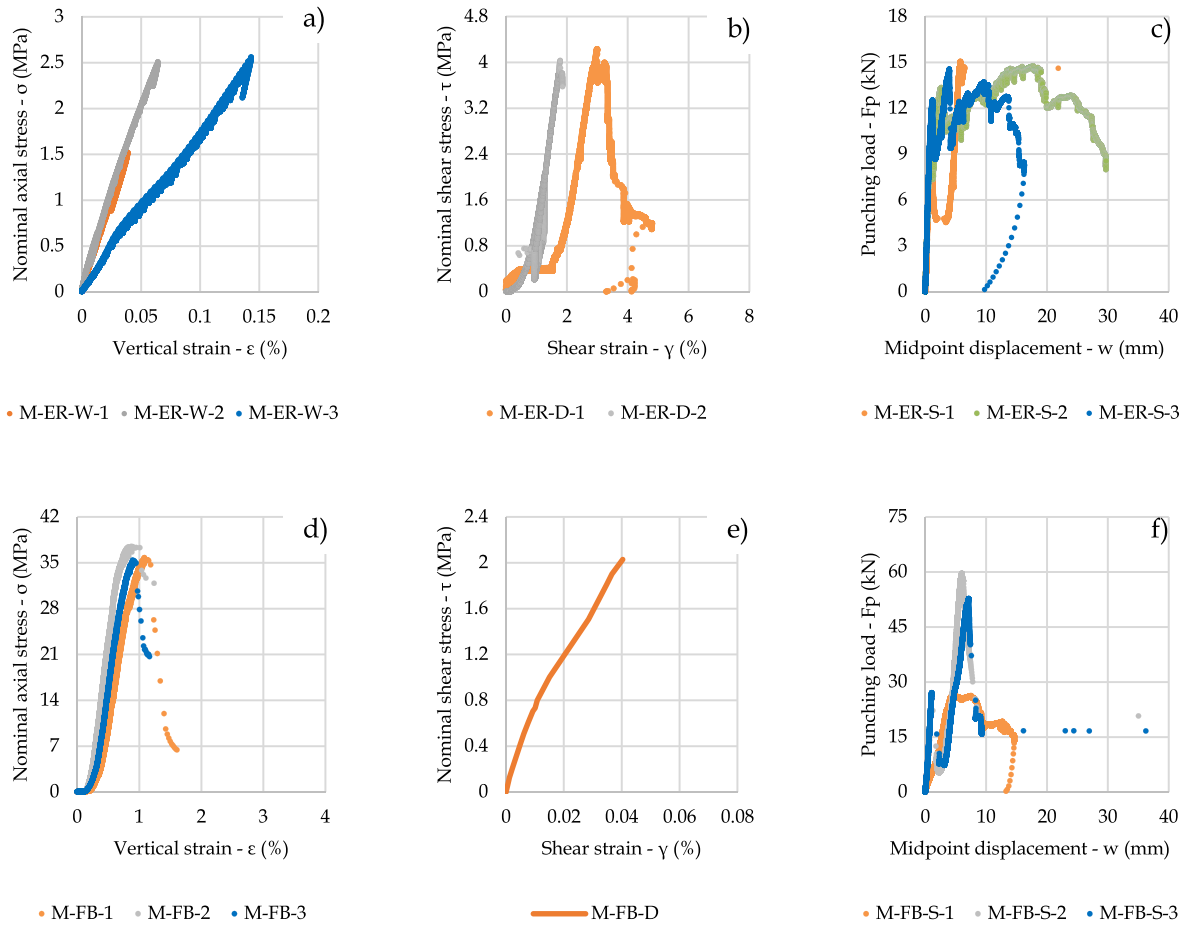

Fig. 13. Mechanical response of macro samples subjected to: (a, d) compression load for M−ER−W, M−FB−W, (b, e) diagonal compression load for M−ER−D, M−FB−D, (c, f) punching load for M−ER−S, M−FB−S. Each subFigure shows the mechanical response of three samples, excluding poor data observed in M−ER/FB-D series.

are obtained from the experimental tests carried out on macro samples presented in Section 2.2.2.1, see Table 2.

The geometry of the H-FEM-M-ER-W corresponds to that of the real M−ER−W, see Table 1. The wall is discretized into 400 hexahedral-shaped 3D elements. The dimensions of each single element correspond to 100 × 100 × 30 mm, see Fig. 8.

In terms of boundary conditions, the H-FEM-M-ER-W is retained by rotationally fixed supports at the bottom, in order to reproduce the real condition seen in the experiment, see Fig. 7a. Instead, the top surface of the H-FEM-M-ER-W is uniformly loaded, in agreement with the experimental configuration observed in Fig. 7a. The load is defined through the application of a prescribed pressure of 1 MPa on the upper surface, see Fig. 9.

3.2. Multi-layered FE model

Differently from the H-FEM, the multi-layered FE model of the Ecorasillas masonry (labeled hereafter ML-FEM-M-ER-W) takes into account the properties of each layer of the real macro samples. In particular, three layers of bricks and two layers of mortars are modeled, in agreement with the real texture showed in the experiment, see the Section 2. Each layer is governed by its own mechanical properties, whose value is measured experimentally or supplied by the producer, see Table 3.

Each layer is discretized in 11, 11 and 1 elements along to the ×, y, z relative coordinate space, respectively, see Fig. 8. The total number of meshing elements is 605, in particular 363 brick and 242 mortar elements. Perfect adherence between layers is assumed. The total number of nodes is 864. The restrain and loading conditions presented in Section 3.1 are adopted for the ML-FEM-M-ER-W as well, see Fig. 9.

3.3. Homogeneous FE model (full-scale analysis)

Among H-FEM and ML-FEM, the former is adopted to analyze the mechanical response of full-scale Catalan vault. The reason is due

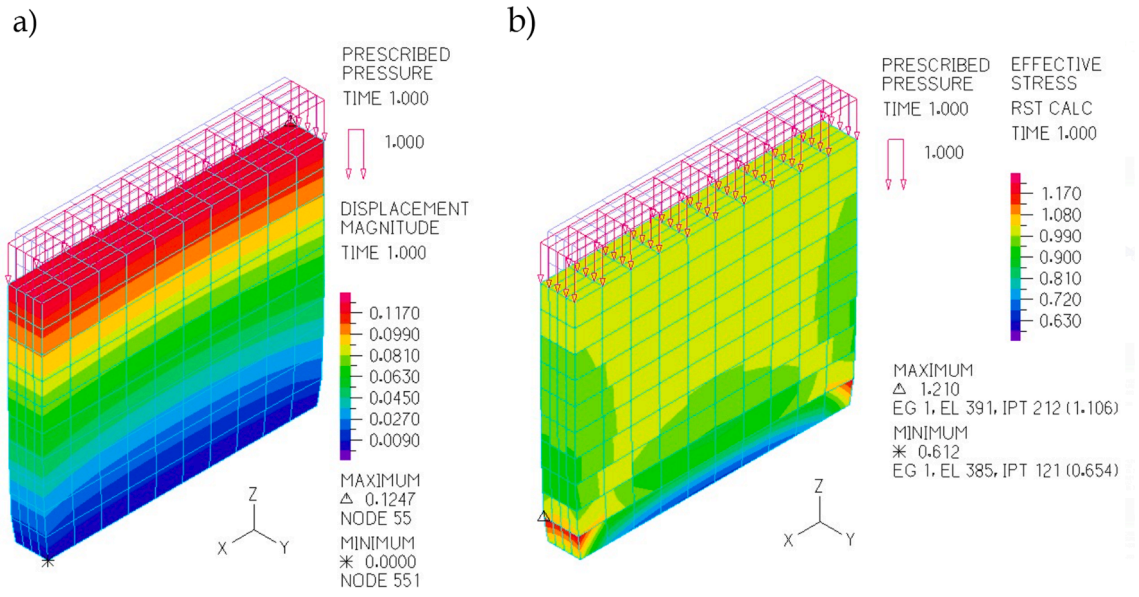

Fig. 14. Compression test simulation on M−ER−W in H-model: (a) z-axis (vertical) displacement magnitude, (b) z-axis (normal) effective stress.

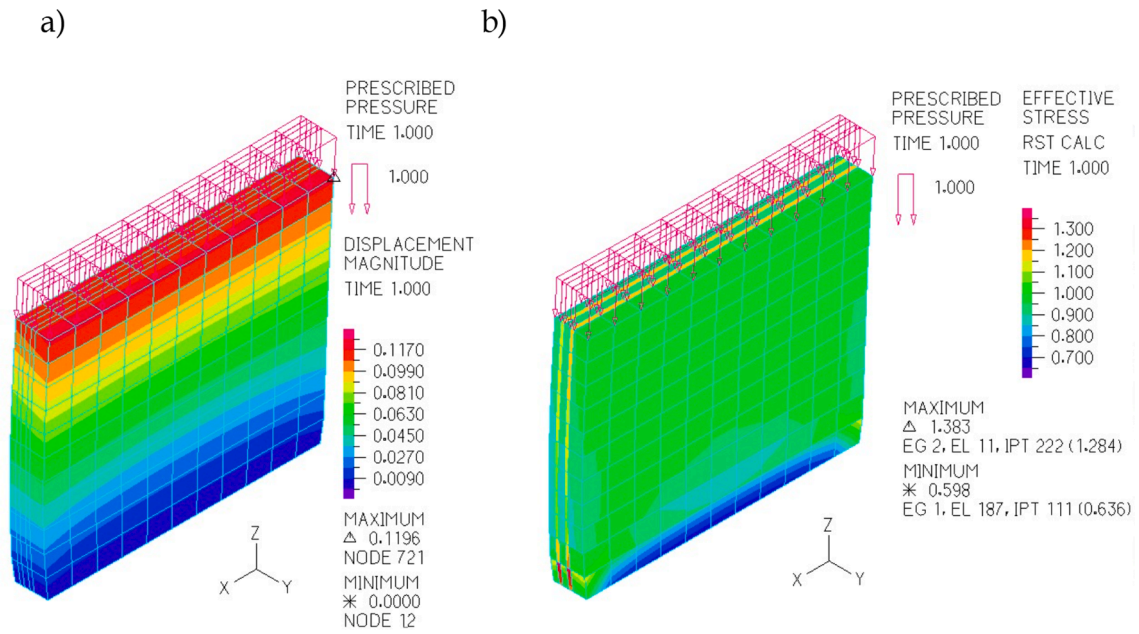

Fig. 15. Compression test simulation on M−ER−W in ML-model: (a) z-axis (vertical) displacement magnitude, (b) z-axis (normal) effective stress.

to the fact that the calibration process of H-FEM has been improved on the basis of the engineering properties measured directly on macro samples. The same approach could be used also for ML-FEM, but it would increase the computational burdens. The geometric properties of the FE vault made of M−ER are listed in Table 5. The material nonlinearity has been taken into account through the Mohr-Coulomb model according to the Eqs 6 and 7 [37]:

$$\frac{m+1}{2}\max(|\sigma_1-\sigma_2|+K(\sigma_1+\sigma_2),|\sigma_1-\sigma_3|+K(\sigma_1+\sigma_3),|\sigma_2-\sigma_3|+K(\sigma_2+\sigma_3))=f_c \tag{6}$$

$$m=\frac{f_c}{f_t};\ K=\frac{m-1}{m+1}$$

where σ_1, σ_2 and σ_3 represent the stresses in the three principal directions, see Fig. 10.

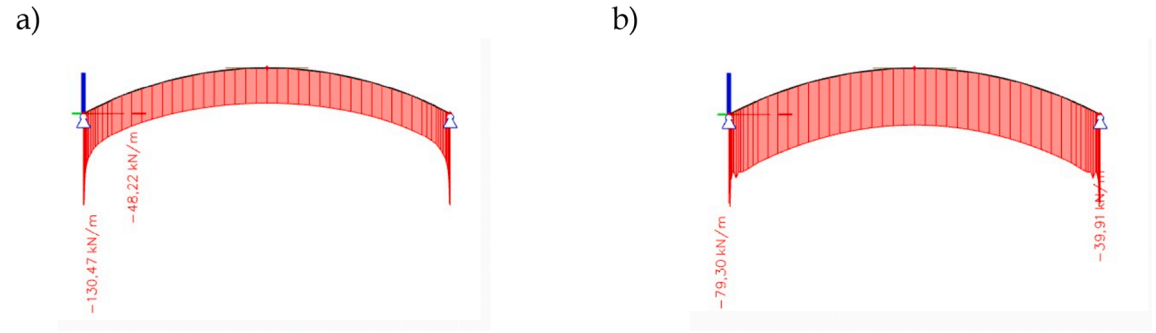

Fig. 16. Coefficient of reduction of the arch effect equal to 1 (a) and 0.0001 (b) on internal axial effort N(x). The vault is subjected to a surface load of 10 kN/m$^{2.}$

The material is supposed to be elasto-plastic, isotropic without hardening. The model calibration parameters are obtained directly from the Ecorasillas masonry tests, except for the f_t, whose value is obtained from the indirect tensile strength (f_b) test. These parameters are summarized in Table 4.

In terms of boundary conditions, the FEM vault can be restrained by rotationally fixed supports at the edge sides, see Fig. 11. This choice permits to reproduce the constraint level observed in the field due to the connection with vertical and horizontal structural members. In terms of loading conditions, first, a surfacing load uniformly distributed is applied just to observe the elastic response of the whole Ecorasillas vault under operational loads. Since the compression strength of M−ER is assumed to be equal to 5.6 MPa, on the basis of the experimental results recorded on M−ER−W, a load magnitude of 10 kN/m^2 is considered for this purpose. Then an assessment of the load bearing capacity is performed by increasing the external surface load to the point that the highest internal stress reaches 5.5 MPa. The behavior of the vault subjected to asymmetrical load of 10kN/m is also analyzed through a H-FEM, labeled H-FEM-A-H, see Fig. 11. Only for this case a comparison is made considering another constraint condition in which also the rotations at the edge sides are fixed (H-FEM-A-F), see Fig. 11.

The central area of the FEM vault is subjected to mesh refinement of 120 mm. Several levels of mesh refinement are adopted at the supports and nodes in order to optimize the computational process. On the supports, an average size of the 2D mesh of 20 mm has been finally adopted. On the 4 extremal nodes of the vault, a circular area with a radius of 250 mm is defined. This circular area encompasses the region of maximum mesh refinement, see Fig. 11. The ratio between the average edge element size in the center of the refinement area and the average preset element size has been set at 0.02. The mesh refinement linearly increases toward the supports.

4. Results and discussions

4.1. Experimental results

The mechanical properties of samples tested in the experimental program presented in Section 2 are listed in Table 6. Results are compared with available data found in Literature. It can be noted that M−ER provides higher mechanical performances than stabilized earth bricks found in Literature, to the point that its performances are comparable to M−FB ones. In Table 6 E_m, G_m, ν, f_c, f_t, f_b, ρ, G_f stand for the Young's modulus, shear modulus, Poisson's ratio, compression strength, direct tensile strength, indirect tensile strength, bulk density and fracture energy, respectively. For M−ER and M−FE, these engineering properties have been directly measured or determined thanks to the experimental campaign previously presented. These experimental data are fundamental to calibrate the models presented in Section 3.

From Table 6 the Young's modulus test on masonry units (M−ER/FB-YM) has been carried out according to [33]. The compression test on masonry units has been set by varying the load direction, see Fig. 4 [30,31]). The properties of commercial mortar M5 used for M−FB are found within the producer's datasheet. M−ER/FB-W are tested under a compression load configuration, see Fig. 13a, 13d. Instead for M−ER/FB-D are tested under a diagonal compression load configuration, see Fig. 13b, 13e. The compression test on M−ER/FB-W permitted to determine the Poisson's ratio, since E_m and G_m, are measured. The fracture energy G_f has been computed by integrating in respect to the deflection-energy absorption path which is plotted in Fig. 13c, 13f on M−ER/FB-S.

Fig. 12 summarizes the failure pattern observed on M−ER/FB-W, M−ER/FB-D and M−ER/FB-S samples subjected to compression, diagonal compression and flexural/punching load, respectively. By observing the out-plane failure in M−ER−W in Fig. 12a it can be stated that failure does not affect all layers. The failure is governed by a delamination process occurring between the first layer and the other ones. This asymmetric out-plane delamination is probably due to the fact that GFRP helps maintaining the second and third layers together. The plane failure observed in Fig. 12a shows that the propagation of the cracks occurs in mortar bonds and not in bricks. In Fig. 12d the failure pattern of M−FB−W sample can be observed. It can be noted that the load bearing capacity of M−FB−W overcomes the maximum load level ensured by the testing machine. For this reason, the wall was cut to 145 × 360 × 360 mm in order to reduce the cross section and repeat the compression test on smaller samples. The out-plane failure affects all layers of bricks. A clear out-plane delamination along the interface mortar-brick is observed while the plane failure occurs in both bricks and mortar joints.

Fig. 12b, 12e show the failure pattern of masonry subjected to diagonal compression load. In particular, for M−ER−D samples a

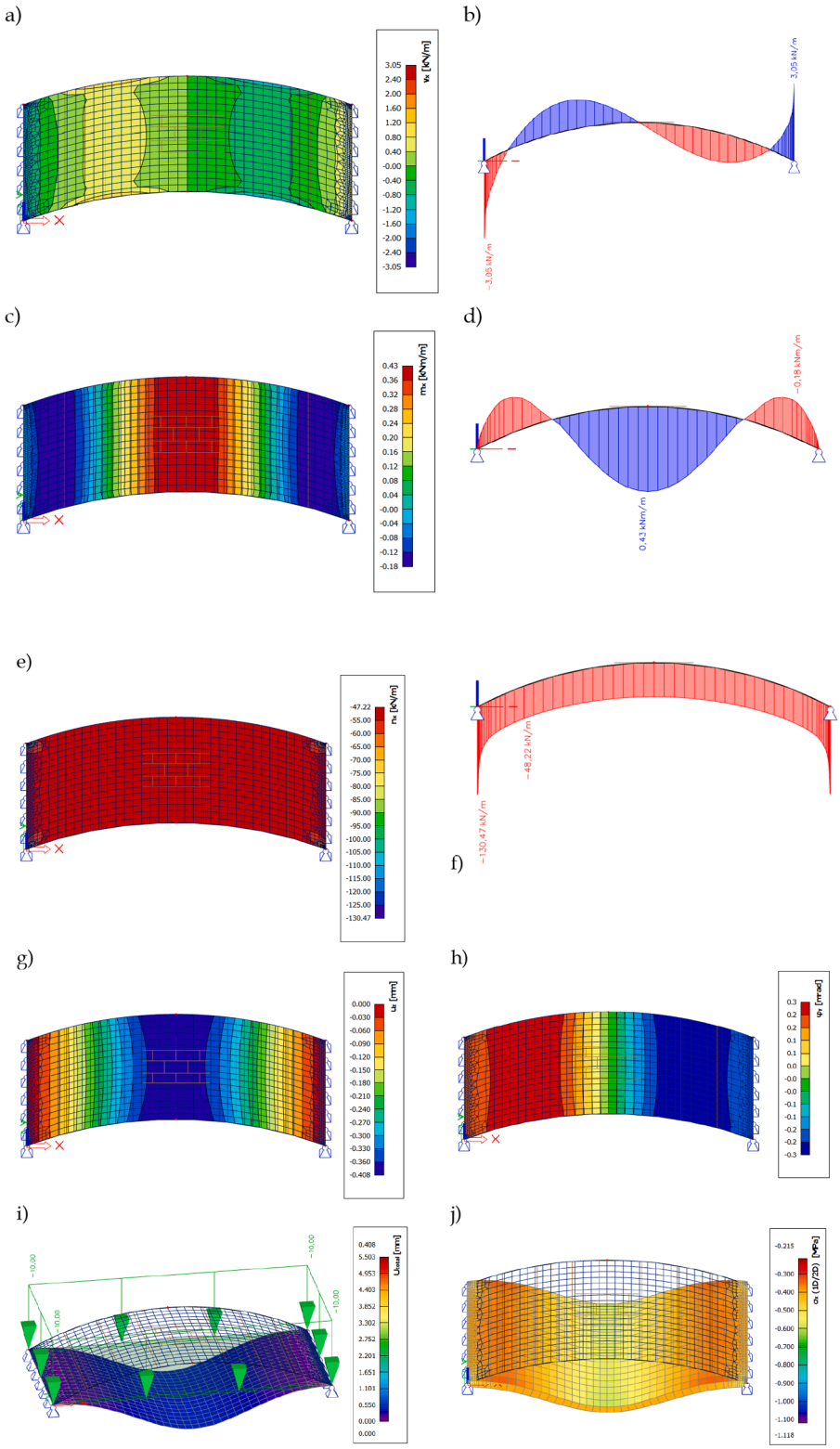

Fig. 17. Computational diagrams of the H-FEM vault subjected to uniform load of 10kN/m^2: (a) internal shear efforts V, (b) internal shear efforts V results on edges, (c) internal axial efforts N, (d) internal axial efforts N results on edges, (e) internal bending efforts M, (f) internal bending efforts M results on edges, (g) global vertical displacement uz, (h) rotation φy, (i) 3D global deformation, (j) internal axial stress σ.

Table 7
Theoretical and computational results.

	Analytical solution	H-FEM Vault model	[1)] Coefficient of Variation (COV) between FEM and analytical solutions (%)
Horizontal reaction (kN)	97	96	1
Vertical reaction (kN)	49	49	0
N(L/2) (kN/m)	−97	−47	106
N(0) (kN/m)	−109	−130	16
V(0) (kN/m)	−2,3	−3,1	25
M(L/2) (kNm/m)	0,44	0,43	2
σ(L/2) (MPa)	−0,31	−0,57	46
w(L/2) (mm)	−0,40	−0,41	2

[1)] COV = (FEM solution – Analytical solution)/FEM solution * 100.

diffusive vertical crack crossing both bricks and joints is observed, but only for the first layer of brick. This observation confirms a different mechanical response between the jointed layers, for different load conditions. A different failure pattern is observed in M−FB−D samples. In the latter the cracking path along the mortar joints does not affect the brick integrity for the entire masonry thickness. Fig. 12c, 12f show the failure pattern of masonry subjected to punching/flexural load. For both M−ER−S and M−FB−S series, a vertical crack path occurs on the edge supported by the steel plate around the samples. Only in M−ER−S the cracks cross the bricks too. Instead, for M−FB−S series the global cracking is due to the delamination between the interface brick – mortar. The same phenomenon is observed in compression and diagonal compression tests. Apparently, the steel grid used in M−FB does not provide overstrength on covered layers, conversely to the GFRP grid used in M−ER.

Fig. 13 points out the mechanical response recorded from the experimental tests previously presented. It can be noted that the load bearing capacity of M−FB series is drastically superior than M−ER series. This large load bearing capacity of M−FB is attributed to the higher performances of FB which had undergone to a clinkerization manufacturing process. However, the failure of M−ER is more ductile than the one of the M−FB. This higher ductility of M−ER failure is probably due to two factors:

- The type of mesh used between the second and third layer in M−FB is a very thin steel grid with low strength compared to the GFRP mesh used in M−ER;
- The crossing bonds of the layers of M−ER favors the cohesive behavior;

4.2. Numerical results

The experimental data showed in Table 6 and presented in Fig. 13 are fitted to be implemented into the FEMs described in the Section 3. In Fig. 14, the H-FEM is used to simulate the deformation process of M−ER−W under an axial compression pressure of 1 MPa. The same scenario is used to simulate the ML-FEM behavior that is presented in Fig. 15. Observing the ML-FEM it is possible to clearly distinguish two different ranges of effective stress along the brick layers. The vertical displacement at the top of the masonry wall resulting in ML-FEM and H-FEM is compared with that measured in the experience. In particular it is 0.16 ± 0.04 mm, 0.12 mm and 0.12 mm for the M−ER−W, H-FEM and ML-FEM, respectively.

Since the accuracy level of both models results the same, the H-FEM is adopted for modeling the Ecorasillas full-scale vault, following the principles presented in Section 3.3. In order to take into account the arch effect, which affects the mechanical response of masonry [44,45], the software proposes two boundary values: 0.0001 and 1. Fig. 16 presents the computational results as the two extreme values are adopted for. In fact, the choice of the coefficient of arch effect may have a relevant influence on the internal load distribution.

4.3. Simulation of structural behavior of ER Catalan vault

In the numerical simulation the arch effect is assumed to be 1 in order to take into account the stress oscillations near to the edges, see Fig. 16. Fig. 17 shows the internal forces, the field of displacements, rotations and the axial 3D stress magnitude for the vault loaded with an evenly distributed load of 10kN/m^2.

The results obtained using the H-FEM approach presented in Fig. 17 are compared with the results of an analytical solution obtained by studying an equivalent beam via the Maxwell-Mohr integral method [46], see Table 7.

By comparing analytical and H-FEM results we can observe a good agreement between all the static reactions, with the exception of the axial and shear effective stress magnitude. These two parameters are strongly influenced by the arch effect. Overall, results in Table 7 confirm the effectiveness of the approach presented in this paper and advocate for further studies on the arch effect parameter.

Fig. 18 show the internal forces, the field of displacements and rotations as well as the axial 3D stress magnitude on ER-based vault according to the H-FEM. The external load is increased in order to reach the compression stress failure recorded in the experimental test on M−ER−W. This value corresponds to about 5.6 MPa, see Fig. 18 and Table 6. The resulting external load provoking the local failure of H-FEM vault is about 110 kN/m^2 which is remarkable for an 8 cm thick Catalan vaults made with Ecorasillas.

Typically, the loads leading to the failure of a vault are asymmetric, promoting the formation of hinges whose position is not easily predictable.

A linear asymmetric load of 10kN/m, acting parallel to the supports, is applied at 1 m (a quarter of the vault span) from the support,

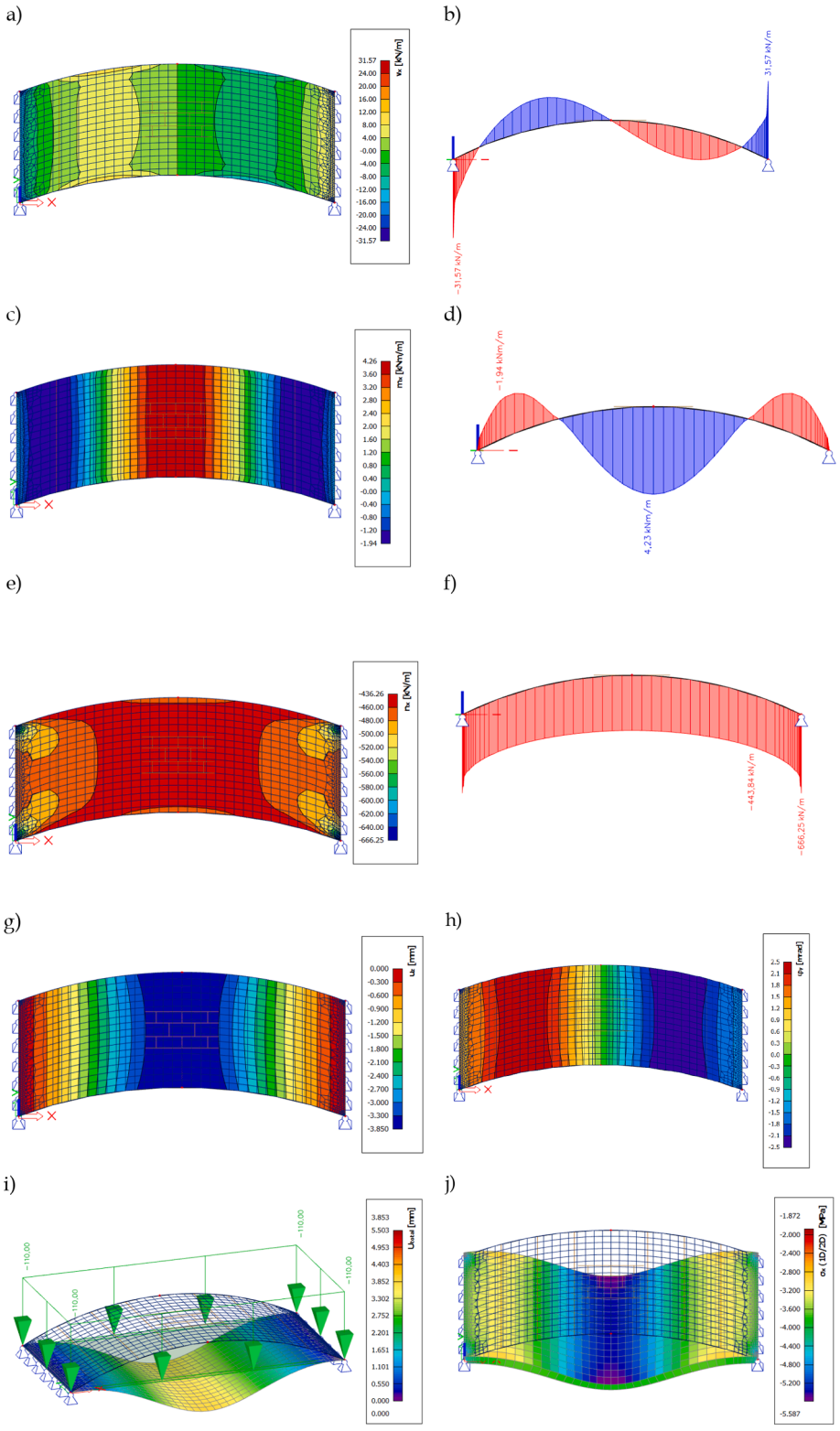

Fig. 18. Computational diagrams of the H-FEM vault subjected to uniform load of 110kN/m^2: (a) internal shear efforts V, (b) internal shear efforts V results on edges, (c) internal axial efforts N, (d) internal axial efforts N results on edges, (e) internal bending efforts M, (f) internal bending efforts M results on edges, (g) global vertical displacement uz, (h) rotation φy, (i) 3D global deformation, (j) internal axial stress σ.

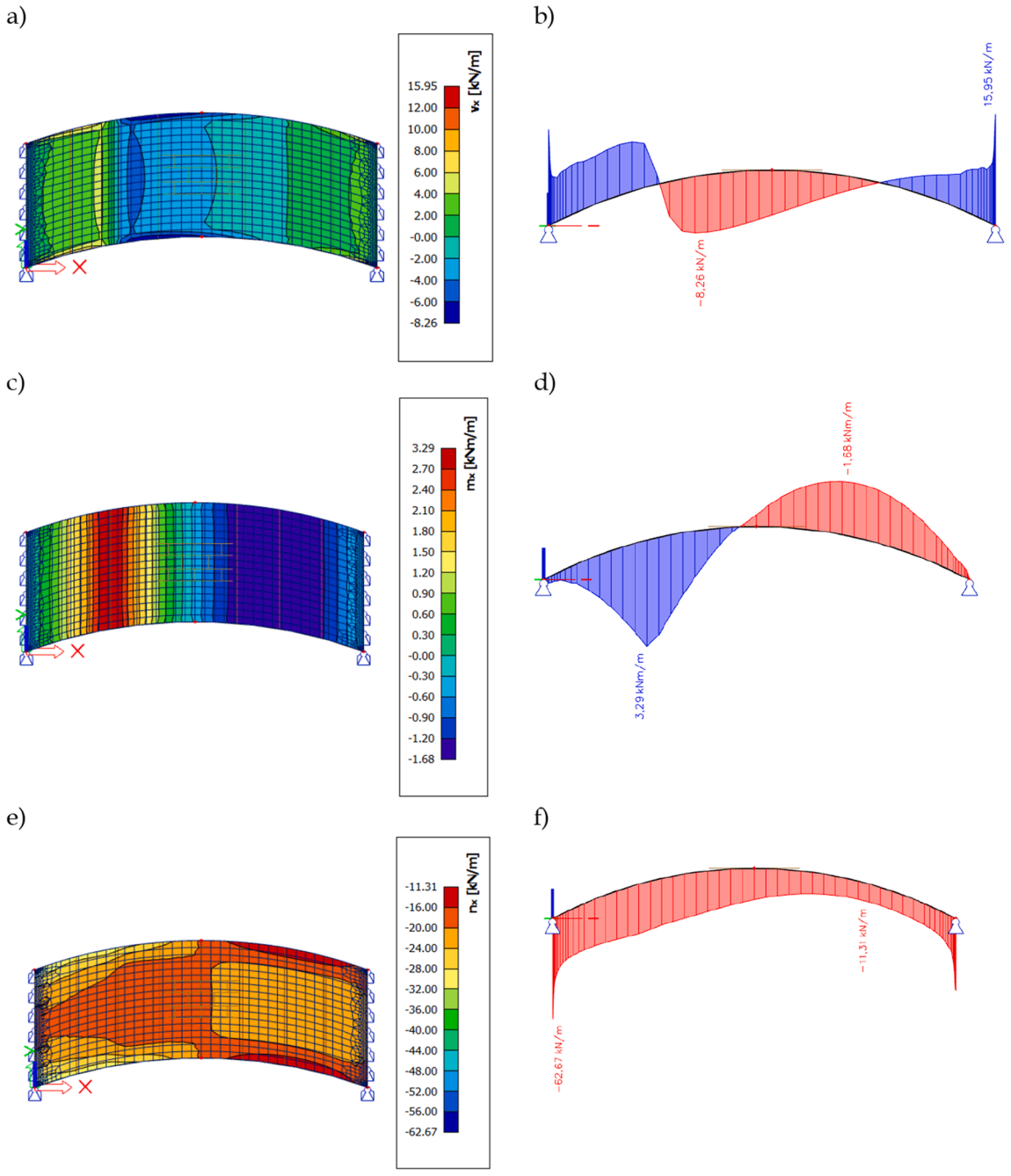

Fig. 19. Computational diagrams of the H-FEM-A-H: (a) internal shear efforts V, (b) internal shear efforts V results on edges, (c) internal axial efforts N, (d) internal axial efforts N results on edges, (e) internal bending efforts M, (f) internal bending efforts M results on edges, (g) global vertical displacement uz, (h) rotation φy, (i) 3D global deformation, (j) internal axial stress σ, (k)horizontal reaction, (l) vertical reaction.

see Fig. 11 and Section 2.2.1.2. Analyzes are made for both H-FEM-A-H and H-FEM-A-F models, that differ in boundary conditions, see Section 3.3. The propagation of the internal stress is showed in Figs. 19 and 20 for the models H-FEM-A-H and H-FEM-A-F, respectively. Table 8 resumes the comparison of internal stress and strain computed by both models.

The pushing effect due to the horizontal constraint reactions R_x is considered unchanged between the two constraint configurations as the percentage variation is 4 % (except at the extremity peak reaching 15 %). For the vertical constraint reactions R_z there are more similar values between the unloading and loading side in the H-FEM-A-F than H-FEM-A-H. Finally, it is noted that by fixing the rotations at the ends, it is possible to have lower M + and higher M-.

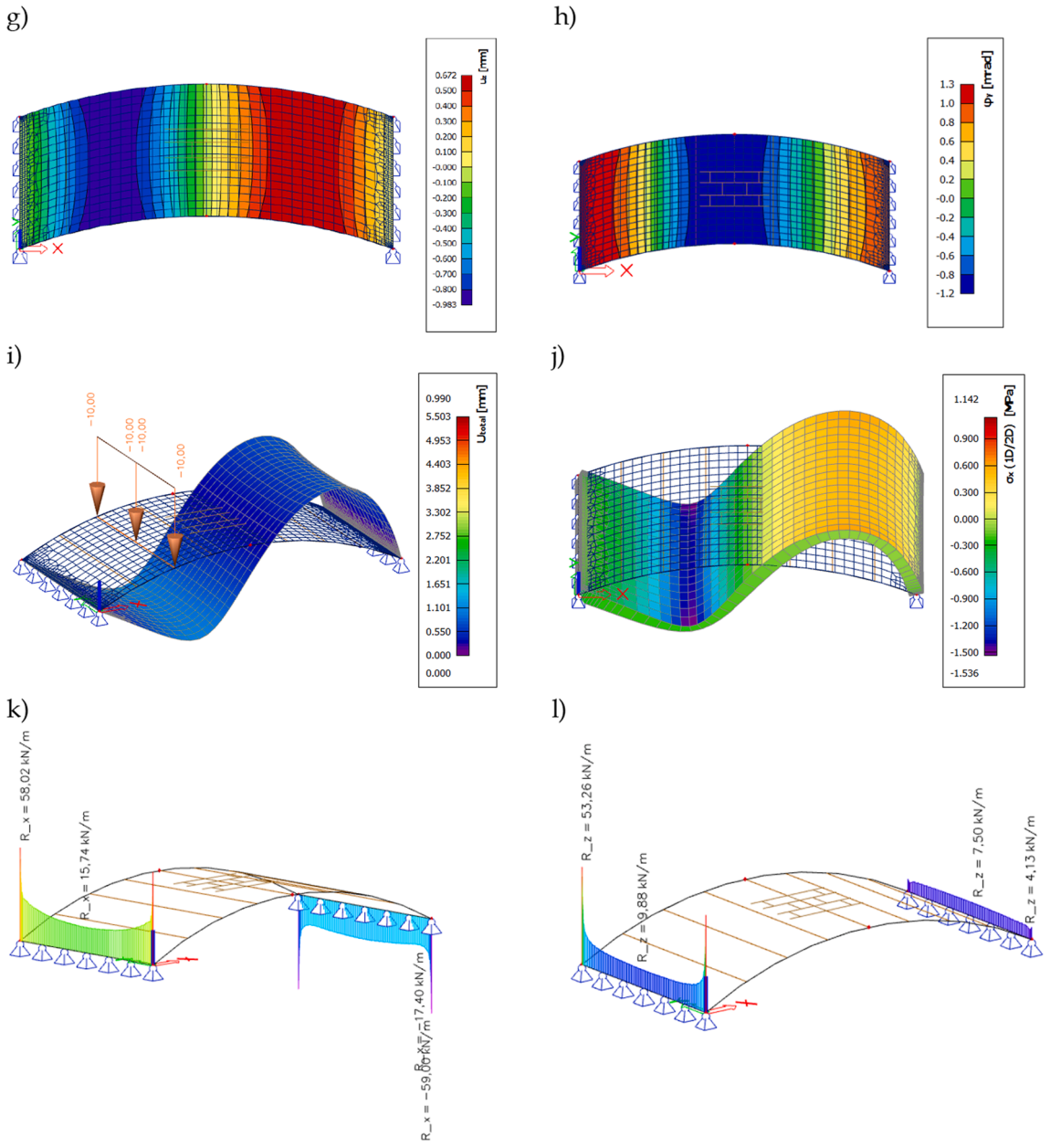

Fig. 19. (*continued*).

In conclusion, since the real constraint at the ends of the vault is a hinge with rotational spring of undefined stiffness, it is advisable during the design phase to consider both of these two possible scenarios (H-FEM-A-F and H-FEM-A-H).

5. Conclusions

The analysis carried out on the masonry based on Ecorasillas masonry (M−ER) confirms that Ecorasillas are suitable to construct safe Catalan vaults. It is worth to remember that the mechanical performances of Ecorasillas vary according to the properties of the excavated earth used to fabricate them. So, a mix design methodology to fabricate Ecorasillas is now of great practical interest.

By comparing the mechanical behavior of M−ER with that of more traditional masonry like clinker bricks (M−FB) three remarkable observations can be drawn:

- M−ER investigated in this work can be efficiently used to construct safe Catalan vaults. The overall strength of the M−ER, although more than sufficient for the structural application, is lower than the one obtained with M−FB;

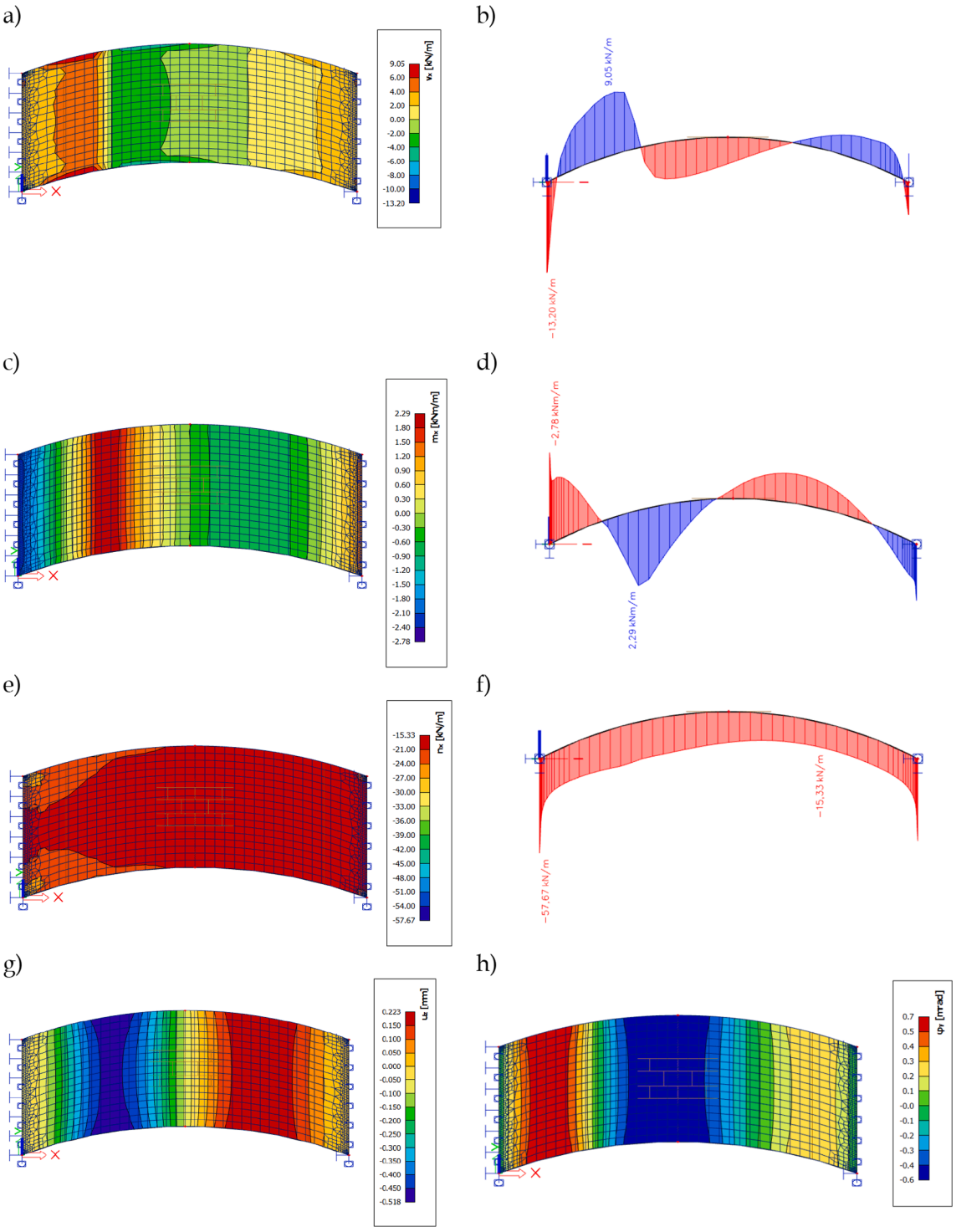

Fig. 20. Computational diagrams of the H-FEM-A-F: (a) internal shear efforts V, (b) internal shear efforts V results on edges, (c) internal axial efforts N, (d) internal axial efforts N results on edges, (e) internal bending efforts M, (f) internal bending efforts M results on edges, (g) global vertical displacement uz, (h) rotation φy, (i) 3D global deformation, (j) internal axial stress σ, (k) horizontal reaction, (l) vertical reaction.

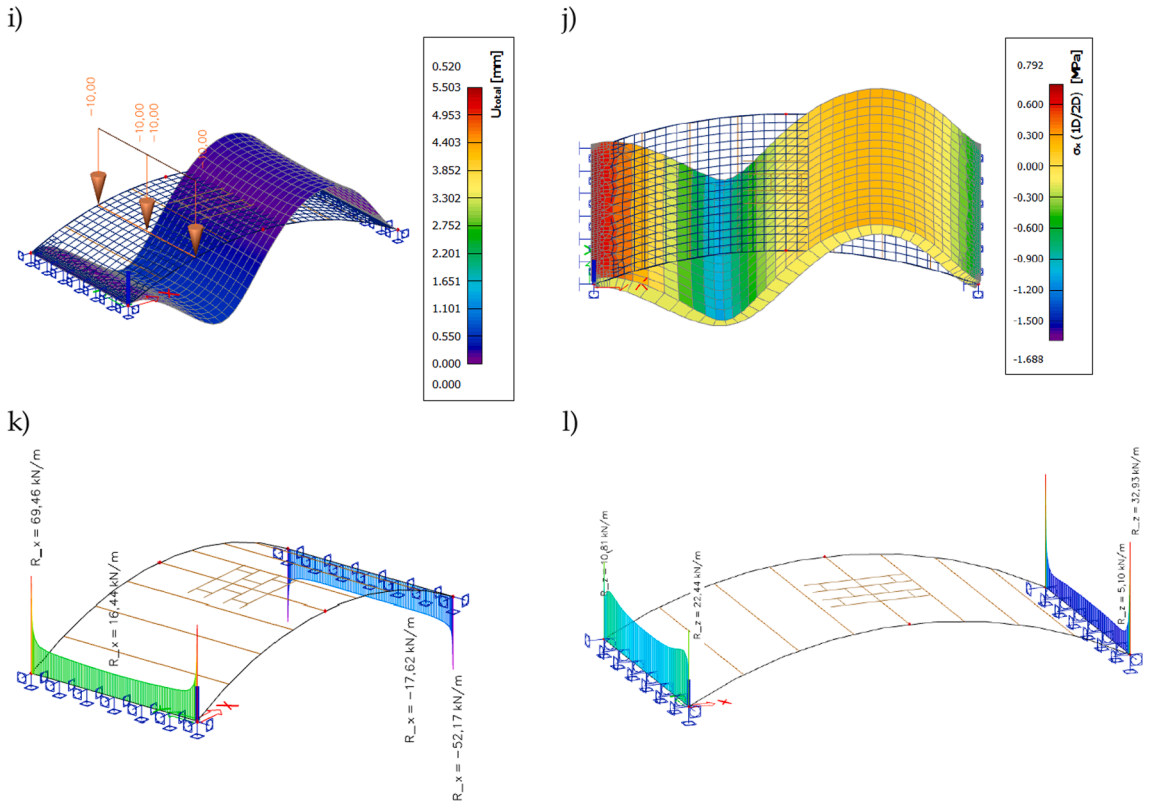

Fig. 20. (*continued*).

Table 8
Internal actions, stress and midspan deflection of Ecorasillas vault (models H-FEM-A-H and H-FEM-A-F).

	H-FEM-A-H	H-FEM-A-F
N(L/2).(kN/m)	−20	−17
N(0).(kN/m)	−62.7	−57.6
V_{max}.(kN /m)	16.0	13.2
$M+_{max}$.(kNm/m)	3.3	2.3
$M-_{max}$.(kNm/m)	1.7	2.8
σ(L/2).(MPa)	−1.5	−1.1
w(L/2).(mm)	0.98	0.52

- However, the higher weight of M−FB clinker bricks makes them not adapted to construct vaults without a formwork, which is possible for M−ER;
- Even though the mechanical performances of Ecorasillas are lower in regard to traditional masonry, they are superior in regard to other earth-based bricks found in Literature. In addition the use of a GFRP mesh drastically improves the ductility of the Ecorasillas Catalan vault. This statement, not yet experimentally validated, has been observed by testing macro-samples.

The experimental campaign here performed permitted to calibrate a numerical model simulating the mechanical behavior of an Ecorasillas Catalan vault on the basis of a multi-level analysis. In the first level, engineering properties of masonry units are used to calibrate the models simulating the mechanical response of the macro elements. In the second level, engineering properties measured by testing macro samples permit to improve the accuracy of the models' calibration. This second calibration reduces the influence of the scale effect and of the boundary conditions on the results of the FEM analyses.

It is however necessary to point out that the Catalan vaults construction techniques has been optimized in centuries of practical experience and research. Therefore, in both types of masonry investigated in this work (M−FB and M−ER), it appeared clearly that modification of the assembly technique of the M−FB elements brought some inconvenient: the uncrossed pattern of the layer for M−FB, combined with the use of a too weak steel mesh implied a more abrupt failure under flexion. A final consideration can be made on the assembly of the ER macro-samples. In this case, opposite to previous testing campaigns, the samples were bonded by masons that are not specialized in the traditional Catalan building techniques. It was observed, during the experimental campaign, that the

samples had a larger propension to the delaminate than similar samples tested in previous campaigns, probably due to the use of a laying and jointing technique of the Ecorasillas that is typical for modern masonry. The use of this modern technique imperiled a good binding of the interlayer mortar to the Ecorasillas, thus favoring the delamination and reducing the overall strength of the elements. Therefore, it is of great importance in the design of vaults to carefully consider the impact of the craftsmanship on the performances of these structures.

Declaration of Competing Interest

The authors declare that they have no known competing financial interests or personal relationships that could have appeared to influence the work reported in this paper.

Data availability

Data used are presented in graphical form in the paper. Some data not presented are confidential

Acknowledgements

Authors gratefully acknowledge the financial support provided by HEIG-VD/HES-SO (Haute Ecole d'ingénierie et de gestion du canton de Vaud – Switzerland) through the projects 98528 NextErathBuilding and 108222 EcoAbri. Authors also acknowledge Ms Louise Mignot and Mr Andrea Curto who actively participated to the experimental campaign and modeling steps cited in this paper.

References

[1] S. Benfratello, G. Caiozzo, M. D'avenia, L. Palizzolo, Tradition and modernity of Catalan vaults: historical and structural analysis, Meccanica dei Materiali e delle strutture 4 (1) (2012).
[2] A. El-Derby, A. Elyamani, The adobe barrel vaulted structures in ancient Egypt: a study of two case studies for conservation purposes, Mediterranean Archaeol. Archaeometry 16 (1) (2016) 295–315.
[3] V. Paris, A. Pizzigoni, S. Adriaenssens, Statics of self-balancing masonry domes constructed with a cross-herringbone spiraling pattern, Eng. Struct. 215 (2020) 110440.
[4] K.I. Nanayakkara, Shell structures: Lessons in structural efficiency for sustainable construction, Struct. Engineer 98 (4) (2020).
[5] G. Castori, A. Borri, M. Corradi, A new method for strengthening tiled vaults: Reinforced Catalan vaulting, in: 9th International Masonry conference 2014 in Guimaraes, 2014.
[6] D. Lopez, M. Domènech Rodriguez, Structural analysis of tile vaulting : method and variables, in: 3rd Biennial Meeting American Construction History, 1850 - 1950, Cambridge MA, 2012.
[7] A. Curto, L. Lanzoni, A.M. Tarantino, M. Viviani, Shot-earth for sustainable constructions, Constr. Build. Mater. 239 (2020) 117775.
[8] F. Laférriere, M. Viviani, Water, soil, construction and demolition: challenges and opportunities, in: Internationa Conference Salus Per Aquas: Ingenii Gratia, 2016.
[9] M. Bacciocchi, V. Savino, L. Lanzoni, A.M. Tarantino, M. Viviani, Multi-phase homogenization procedure for estimating the mechanical properties of shot-earth materials, Compos. Struct. 295 (2022) 115799.
[10] S. Vantadori, A. Zak, Ł. Sadowsky, C. Ronchei, D. Scorza, A. Zanichelli, M. Viviani, Microstructural, Chemical and Physical Characterisationof the Shot-Earth 772, Constr. Build. Mater. 341 (127766) (July 2022) 25.
[11] M.S. Zami, Counterbalancing benefits and drawbacks of contemporary stablised earth construction by construction professionals, Archnet-IJAR, Int. J. Archit. Res. 5 (2011) 49–62.
[12] L.D. Lopez, T. Van Mele, P. Block, Tile vaulting in the 21st century, Informes de la Construccion 68 (2016).
[13] D.P. Billington, Thin shell concrete structures, McGraw-Hill, in New York, 1965.
[14] J. Heyman, Equilibrium of shell structures, Oxford University Press, 1977.
[15] P. Block, T. Ciblac, J.A. Ochsendorf, Real-time limit analysis of vaulted masonry buildings, Comput. Struct. 84 (29–30) (2006) 1841–1852.
[16] M.H. Ramage, Catalan vaulting in advanced materials: new approaches to contemporary compressive form, Master thesis, Massachusetts institute of technology, 1995.
[17] T. Ciblac, The theories of graphic statics revisited by digital approaches. From parametric structural evaluation to morhogenesis, in: SHS Web of Conferences 82, GSA, ENSA Paris-Malaquais, 75006 Paris, France, 2020.
[18] C. Fivet, Constraint-based graphic statics, PhD Thesis, UCL - Université Catholique de Louvain, 2013.
[19] C. Fivet, D. Zastavni, A fully geometric approach for interactive constraint-based structural equilibrium design, ComputerAidded Des. 61 (2015) 42–57.
[20] R. Gulli, Le volte in folio portanti: Tecnica costruttiva ed impiego nell'edilizia storica e moderna, in: Atti del I Convegno Nazionale Manutenzione e Recupero nella Città Storica ARCO, Rome, Italy, 1993.
[21] B. Pulatsu, E. Erdogmus, P.B. Lourenço, R. Quey, Simulation of uniaxial tensile behavior of quasi-brittle materials using softening contact models in DEM, Int. J. Fract. 217 (1-2) (2019) 105–125.
[22] A. Pascuzzo, F. Greco, L. Leonetti, P. Lonetti, A. Pranno, C. Rochei, Investigation of mesh dependency issues in the simulation of crack propagation in quasi-brittle materials by using a diffuse interface modeling approach, Fatigue Fract. Eng. Mater. Struct. 45 (3) (2022) 801–820.
[23] A. Mohammed, T.G. Hughes, A. Mustapha, The effect of scale on the structural behaviour of masonry under compression, Constr. Build. Mater. 25 (1) (2011) 303–307.
[24] S. Huerta, in: Essays on the History of Mechanics, Birkhäuser Basel, Basel, 2003, pp. 89–134.
[25] L. Palizzolo, S. Benfratello, A. Caffarelli, F. Giambanco, R. Urso, "Bóvedas tabicadas: experimental and numerical analysis, in: High Performance Structuers and Materials IV, Algarve (Portugal), 2008.
[26] P. Christian, "Christian Pottgiesser architecturespossibles," Ault Common Home, [Online]. Available: http://www.pottgiesser.fr/cpap-ongoing.html. [Accessed 2020].
[27] K.A.J. Ouedraogo, J.-E. Aubert, C. Tribout, G. Escadeillas, Is stabilization of earth bricks using low cement or lime contents relevants? Constr. Build. Mater. 236 (2020) 117578.
[28] En,, 77–1 + A1, "Specification for masonry units - Part 1: Clay masonry units,", CEN EN (2015).
[29] M. Dejong, M. Ramage, B. Travers, S. Terry, Testing and Analysis of Geogrid-reinforced Thin-shell Masonry, in: 35th Annual Symposium of IABSE/52nd Annual Symposium of IASS/6th International Conference on Space Structures, London (UK), September 2011.
[30] AFNOR - 13 901 XP P, "Briques et blocs de terre crue pour murs et cloisons - Définitions - Spécifications - Méthodes d'essai - Conditions de réception," 2022.

[31] A.W. Bruno, D. Gallipoli, C. Perlot, J. Mendes, Mechanical behaviour of hypercompacted earth for building construction, Mater. Struct. 50 (2) (2017).
[32] EN 1015-11, "Methods of test for mortar for masonry - Part 11: Determination of flexural and compressive strength of hardened mortar," CEN, 2019.
[33] EN 12390-13, "esting hardened concrete - Part 13: Determination of secant modulus of elasticity in compression, in: CSN, 2013.
[34] ASTM E519/E519M-10, Standard test method for diagonal tension (shear) in masonry assemblages, ASTM, 2015.
[35] K.-J. Bathe, Finite element procedures, Second ed., 2014.
[36] 2022. [Online]. Available: https://www.scia.net/fr/software/scia-engineer.
[37] J.F. Labuz, A. Zang, Mohr-Coulomb failure criterion (2012).
[38] D. Lopez, M.D. Rodriguez, M.P. Fernandez, Brick-topia, the thin-tile vaulted pavilon, Case Stud. Struct. Eng. 2 (2014) 33–40.
[39] G. Creazza, R. Matteazzi, A. Saetta, R. Vitaliani, Analyses of masonry vaults: a macro approach based on three-dimensionale damage model, J. Struct. Eng. 128 (2002).
[40] S.P. Narayanan, M. Sirajuddin, Properties of Brick Masonry for FE modeling, Am. J. Eng. Res. 1 (2013) 6–11.
[41] G. Bei, I. Papayianni, Compressive strength of compressed earth block masonry, Trans. Built Environ. 66 (2003) 367–376.
[42] L. Miccoli, U. Muller, P. Fontana, Mechanical behaviour of earthen materials: A comparison between earth block masonry, rammed earth and cob, Constr. Build. Mater. 61 (2014) 327–339.
[43] E. Hany, N. Fouad, M. Abdel-Wahab, E. Sadek, Investigating the mechanical and thermal properties of compressed earth bricks made by eco-friendly stabilization materials as partial or full replacement of cement, Constr. Build. Mater. 281 (2021) 122535.
[44] A.W. Hendry, B.P. Sinha, S.R. Davids, An introduction to load-bearing brickwork design, Ellis Horwood Limited, New York, 1981.
[45] A. W. Hendry, Structural brickwork, London: McMillan Press, 1981.
[46] I.A. Karnovsky, O. Lebed, Advanced Methods of Structural Analysis, Springer, New York, NY, 2010.